UNIVERSITÉ PARIS XI
UFR SCIENTIFIQUE D'ORSAY

École Doctorale Particules, Noyaux et Cosmos

Laboratoire de l'accélérateur linéaire

THÈSE DE DOCTORAT

présentée par : **Mathieu Benoit**

soutenue le : **13 Juin 2011**

pour obtenir le grade de : **DOCTEUR EN SCIENCES DE L'UNIVERSITÉ PARIS XI ORSAY**

Spécialité : **Physique des Particules**

Étude des détecteurs planaires pixel durcit aux radiations pour la mise-à-jour du détecteur de vertex d'ATLAS

THÈSE DIRIGÉE PAR

M. Lounis Abdenour — *Maitre de Conférence, LAL*

RAPPORTEURS

M. Auger Etienne — *Titre, Etablissement*
M. Casse Gianluigi — *Professor, University of Liverpool*

EXAMINATEURS

M. Fournier Daniel — *Titre, Etablissement*
M. Gossling Claus — *Titre, Etablissement*
M. Wormser Guy — *Titre, CNAM*

"citation"
Auteur

Remerciements

Ici les remerciements

Résumé

Ici le résumé

Mots clés : Mots clés

Abstract

Here the abstract

Keywords : keywords

Table des matières

Liste des tableaux

Table des figures

Introduction

ici l'introduction

Chapitre 1

The ATLAS Upgrade project

texte...

1.1 The Inner detector

texte...

1.2 The calorimeters and Muon Chambers

texte...

1.3 THe SLHC project

texte...

1.3.1 Phase 1 : The Insertable b-layer (IBL)

texte...

1.3.2 Phase 2 : Upgrade for high luminosity

Chapitre 2

Principles of Silicon pixel sensors

Silicon-based detector have been used for the last 60 years as an efficient mean to detect the presence of charged particles. Gold contact barrier, then p-n junction diodes were used between 1955 and 1965 as an efficient small size spectroscopic sensor to measure the ionizing energy deposition of β particles in silicon. The first HEP experiment to make a wide use of silicon as a tracking detector was CERN's NA11 and NA32 experiments Hartmann [2009]. The strip sensors used in their tracking system shown the possibility of large scale usage of these sensors in tracking applications in HEP.

Nowadays, the wide use of silicon diode based sensors allowed for the development of very sophisticated detectors used in large scale experiments where high resolution tracking of charged particles is required. Their increased exposure to radiation in high luminosity experiments due to their proximity to the interaction points remains a challenge as aging effects have been observed with increasing exposure to high energy particles. In this chapter I will describe the basic semiconductor physics behind the p-n junction based detectors and the mechanism that allow them to be used as efficient radiation detection devices. I will describe the ATLAS Hybrid planar pixel sensor which is the main study subject of this thesis. A quick survey of the concurrent technologies will be presented.

Finally, the physics behind the aging effects of silicon detectors due to exposure to radiation will be described. The empirical models developed in the recent years will be compared to the microscopic effects of radiation damage of silicon to provide an explanation of the behavior observed in irradiated silicon sensors.

2.1 The physics of Silicon

2.1.1 Semiconductors properties

Silicon used in particle detection is a semiconductor with a face-centered cubic crystalline structure, as shown in figure 2.1.

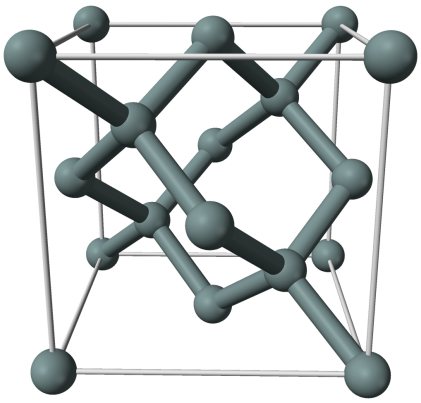

FIGURE 2.1 – Unit cell of silicon crystalline structure

The periodic nature of the silicon crystal lattice create the conditions for the electrons of the silicon atoms to arrange, in the energy-impulsion domain, in a band structure, as seen in figure 2.2 with forbidden zones where an electron cannot be found. This energy region where electrons cannot be found is called the bandgap. The height of this region is a unique property of each semiconductor.

The valence electrons of the silicons atoms are distributed between the conduction band and the valence band. The electrons in the conduction band are weakly bound to the lattice and can freely move through the material while the valence electrons are constrained to stay close the lattice structure. The Pauli exclusion principle forbids that two fermions, such as electrons, lie in the same energy-impulsion state. The energy distribution of this gas of fermions can be best described by the Fermi-Dirac distribution function (eq. 2.1) :

$$n_i = \frac{g_i}{e^{\frac{E_i - \mu}{k_B T}} + 1} \tag{2.1}$$

where g_i is the degeneracy factor of the energy state and μ is the Fermi-Dirac quasi-energy

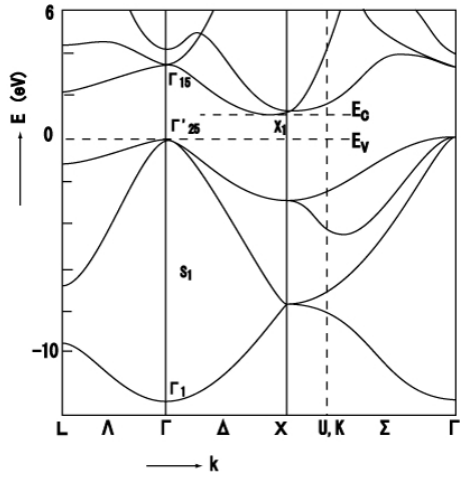

FIGURE 2.2 – Silicon band structure in the energy-impulsion domain

level. At low temperature ($k_BT << \mu$), μ is the energy level under which all state are occupied. At high temperature ($k_BT >> \mu$),μ is the energy level over which a state has only a probability of 50% of being occupied. The Fermi-Dirac distribution at different temperature is shown in figure 2.3.

This principle leads to the introduction of a virtual particle, the hole, as the carrier of the "absence of an electron" in the valence band of silicon. The addition of impurities to the crystalline structure modify the macroscopic properties of silicon. When impurities inserted in the crystal structure have a number of valence electrons (N_{ve}) different than 4, for silicon, extra electrons ($N_{ve} > 4$) or holes ($N_{ve} < 4$) are introduced in the band structure. The hole introducing dopant is called an acceptor and is found in p type silicon. The electron introducing impurities are called donors and are found in n type silicon. Both type of dopant can be present in silicon and will compensate each other in such way that only the net dopant concentration will be electrically active. In n type and p type semiconductors , the Fermi-Dirac quasi-energy level is found respectively close to the conduction or the valence band. The additional carriers will fill energy states not occupied in the intrinsic silicon modifying the position of the Fermi-Dirac quasi-energy level. At high temperature typical of the operation of silicon sensors, most of the impurities additional carriers are added to the cloud of free carriers in the silicon crystalline structure, increasing the amount of carriers available for conduction. In highly doped silicon ($N_{D,A} > 10^{18} cm^{-3}$),

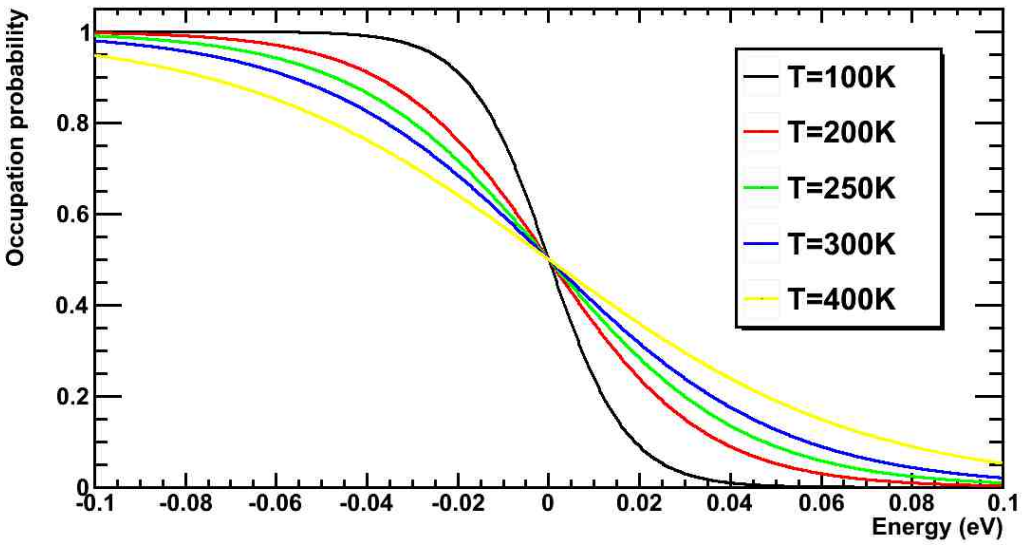

FIGURE 2.3 – Fermi-Dirac Distribution, $\mu = 0$, $g_i = 1$

the amount of additional carriers is such that energy levels in the valence band, for holes, or in the conduction band, for electrons, have a probability close or equal to 1 of being occupied. This lead to high conductivity of the material even at low temperature.

2.1.2 Charge transport

The dynamics of the carriers inside silicon can be described by the drift-diffusion equations (eq. 2.2 and 2.3) coupled to the Poisson (eq. 2.4) Peter and Cardona [2003] :

$$\frac{dp}{dt} = \nabla \cdot D_h \nabla p + \nabla \cdot (p\mu_h \vec{E}) + G_h - R_h \tag{2.2}$$

$$\frac{dn}{dt} = \nabla \cdot D_e \nabla n - \nabla \cdot (n\mu_e \vec{E}) + G_e - R_e \tag{2.3}$$

$$-\nabla^2 V = \nabla \cdot \vec{E} = \frac{\rho}{\epsilon} \tag{2.4}$$

where p and n are respectively the density of holes and electrons in $[\frac{1}{cm^3}]$, D in $[\frac{cm^2}{s}]$, their respective diffusion coefficient, μ the mobility in $[cm^2/V/s]$. G is the generation rate

and R, the recombination rate, both in $[1/cm^3/s]$. The h and e subscript respectively design holes and electrons. ρ is the net charge density in $[C/cm^3]$, where C are Coulomb.

Mobility of charge carriers in silicon is influenced by the magnitude of the parallel electric field in which it is drifting. In a high electric field, free carrier's energy loss by inelastic scattering in the crystal lattice will balance with the energy gained from acceleration in the electric field. This leads to the saturation of the carrier's speed Peter and Cardona [2003]. This effect can be expressed in terms of a variation of the mobility (μ) as a function of the parallel electric field magnitude Caughey and Thomas [1967]. Equation 2.5 and 2.6 show the typical expression used to model the parallel field dependence of mobility in Silicon.

$$\mu(E) = \mu_0(\frac{1}{1 + (\frac{\mu_0 E}{v_{sat}})^{\beta}})^{-\beta} \tag{2.5}$$

$$v_{sat} = \frac{\alpha}{1 + \theta e^{\frac{T_L}{T_{nominal}}}} \tag{2.6}$$

Where T_L is the lattice temperature. Typical values used for this model are shown in table 2.1.

TABLE 2.1 – Parallel field dependence mobility model parameters

Parameter	Electrons	holes
μ_0 $(cm^2/Vs$ at $300K)$	1400	450
β	2.0	1.0
α (cm/s)	2.4×10^{-7}	2.4×10^{-7}
θ	0.8	0.8
$T_{nominal}$ (K)	600	600

Generation/Recombination terms are important to describe the behavior of silicon detectors. Generation is responsible for leakage current present in detectors under bias. Recombination occurs between free carriers and its rate is proportional to the concentration of the most rare carrier. Silicon being an indirect gap semiconductor, generation and recombination occurs mostly through the defect states that are present in the bandgap of Silicon. A model that can be used to evaluate this term is the Shockley-Read-Hall Generation-Recombination Peter and Cardona [2003] model, which describe generation-recombination

in indirect-bandgap semiconductors as Silicon. This model approximates that the transition of carriers in the bands occurs through a single trap level located at midgap, E_{trap} with an interaction with a phonon.

2.1.3 The pn junction

When two regions of silicon containing different concentration of free carriers are put into contact, we form a junction if the two region are respectively of p and n type. At the contact region, the excess holes and electrons present create an electric field dragging free carriers on the other side of the junction . A space-charge region is created at the junction where the electric field is present. The rate of carriers entering the space-charge region by diffusion from the doped region is equal to the rate of carriers leaving this region by drifting in the electrical field built by the difference of carrier concentration on each side of the junction. A zone with very low concentration of free carriers that is created at the junction is called the depletion zone. The only free carriers present are coming from the thermally generated carriers created to replace the carriers drifting away in the electric field. The application of an additional electric field through electrodes in contact with each side of the junction will modify this equilibrium by dragging carriers from the doped regions away or within the junction and modify the width of the depletion zone.

The pn junction can be biased in two different manners, as illustrated in figure 2.4. If a negative voltage is applied on the n side and a positive voltage on the p side of the junction, the depletion zone tends to shrink and the electric field in the depletion zone is reduced, allowing more charge to cross the potential barrier and diffuse in the opposite side of the junction. This results in a reduction of the apparent resistance of the pn junction and a non-linear exponentially increasing current. In the opposite case , the depletion region will expand away from the junction and the electric field increases as the amount of space charge becomes more important. The only current flowing through the junction is the diffusion current from each depletion region edges, which saturates with distance, and the generation/recombination current from the depletion region.This result in an apparent increase of the resistance of the pn junction and results in a saturation of leakage current. Figure 2.5 show the typical Current versus bias of a pn junction.

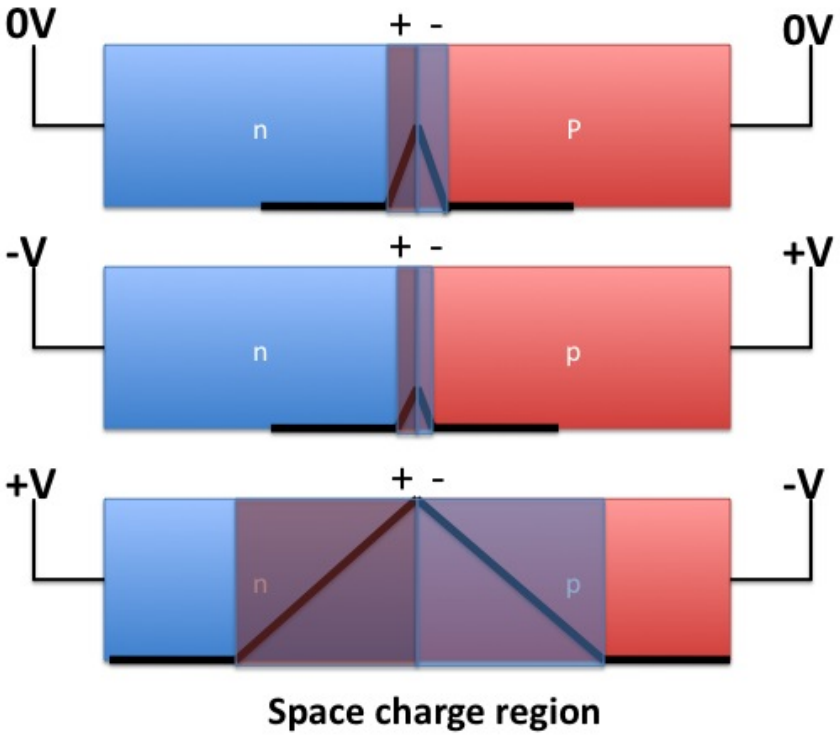

FIGURE 2.4 – The three possible state of a pn junction : at rest (top), forward bias (middle), reverse bias (bottom). The depletion region relative size is shown on the figure with the space-charge sign of each zone of the diode.

The depleted zone in reverse bias mode represent the volume where particle energy deposition can be detected as carriers generated through this process can drift into the electric field and generate a signal. The width of the depletion zone can be calculated using equation 2.7 Knoll [2010].

$$d = \sqrt{\frac{2\epsilon V}{eN}} \tag{2.7}$$

Where ϵ is the electrical permittivity in silicon, V the applied bias voltage, e the electron charge and N the dopant concentration in the region where dopants are less concentrated.

These properties of silicon can be used to build devices with interesting characteristics

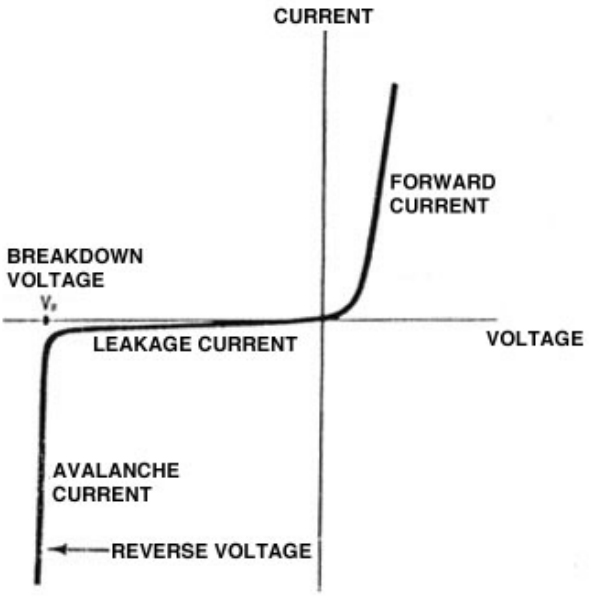

FIGURE 2.5 – !!! Mettre belle Mesure ICI!!!!! Typical pn junction current versus bias characteristics.

for radiation detection. Further discussion on the physics of silicon can be found in chapter 3 of this thesis. A mathematical treatment of the pn diode equation presented here can be found in the annex.

2.1.4 Magnetic field effects

Semiconductors sensors for particle tracking application are often used in a magnetic field to allow the measurement of the transverse momentum of incoming particles. While the presence of a field modify the behavior of the detectors, they can be operated in intense magnetic field without hurting the detector performances. The carriers inside the magnetic field are subject to the Lorentz force (equation 2.8), where is the velocity of the carrier and B the magnetic field intensity.

$$\vec{F} = q(\vec{E} + v \times \vec{B}) \tag{2.8}$$

The additional component of the force due to the magnetic field presence leads to carriers drifting away from the electric field lines with an angle determine by equation 2.9 Lutz [2007], where *theta* is the angle between the electric field and the actual carrier drift

trajectory and $\mu^H_{p,n}$ is the Hall mobility, which differs from normal mobility because of the effects of the presence of the magnetic field.

$$tan\theta_{p,n} = \mu^H_{p,n} B \tag{2.9}$$

2.2 Radiation detection

2.2.1 The energy deposition process

The reverse bias operation mode of the silicon pn diode presents interesting characteristics for charged particle and x-ray detection. The radiation interacting with silicon diodes through ionizing process such as photoelectric effect, Compton scattering and through transfer of energy to the bound carriers by coulombial scattering generate an amount of free carriers in electron-hole pairs, proportional to the amount of energy deposited in the diode through these ionizing processes. The mean amount of carriers generated in such process ($N_{e,h}$) is given by eq. 2.10 where E_d is the deposited energy and E_g is the pair production energy, 3.64eV for silicon.

$$N_{e,h} = \frac{E_d}{E_g} \tag{2.10}$$

The pair production process is an almost stochastic one, but the pair production process is not independent from pair to pair as the energy deposition occurs in a cascade of energy transfers from the incoming particle to the carriers and from excited carriers to other carriers. This correlation between the different pair production events gives rise to the Fano factor (F=0.01 for silicon Mazziotta [2008])in the intrinsic energy resolution equation (eq. 2.11) of semiconductor sensors to account for the lower standard deviation observed with regard to the Poisson predicted standard deviation.

$$\sigma_{Si} = \sqrt{F N_{e,h}} \tag{2.11}$$

In a silicon diode used as a particle sensor, a diode is biased and the depleted region represents the active detection region. A particle deposit its energy and a cloud of

electron-hole pairs are created. Following the electric field, they drift toward the electrodes generating an additional current in the diode that can be measured using detection electronics, as shown in figure 2.6.

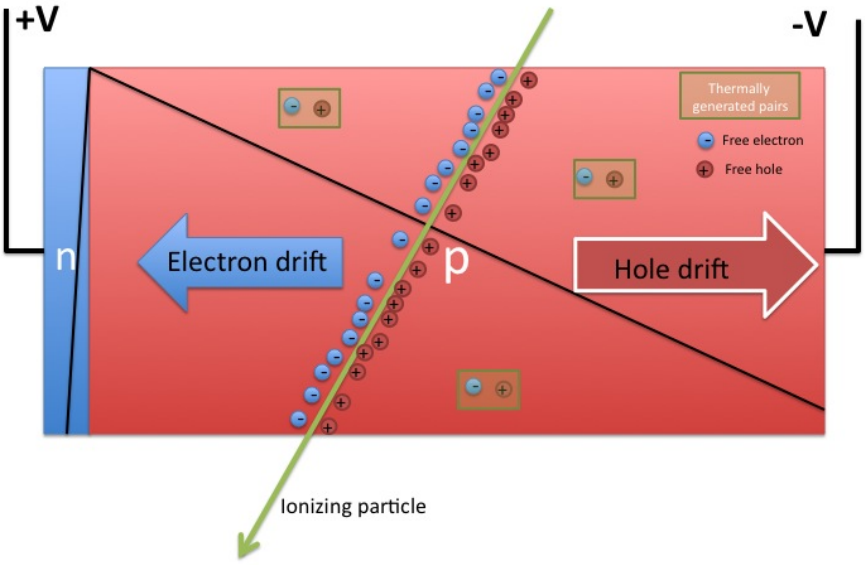

FIGURE 2.6 – Schematics of ionizing particle detection in a reverse biased diode. The free electron hole pairs produced by the particle energy loss drift in the electric field and produce a current in the diode. Thermally generated (green boxes) are also generated in the depleted zone of the diode.

The low reverse biased diode leakage current represent an advantage of silicon sensors. This leakage current is caused by electron-hole pairs being thermally generated in the the depleted zone of the diode. These pairs also induce signal on the read-out electrode and are emitted randomly thus subject to statistical variations. This increases the noise in the sensor and low leakage current present in reverse-biased diodes makes it a perfect detection medium for ionizing radiation.

2.2.2 Signal formation

The signal induced on a readout electrode is not due to the collection of the free carriers themselves. The charge's electric field flux inside the readout electrode varies as the charge

drift into the sensor and displacement current is created and generate the detectable signal. The real signal can be calculated using the Ramo theorem Ramo [1939], as shown in 2.12.

$$Q_k = \sum_i q_i \phi_k(\vec{r_i}_{final}) - \sum_i q_i \phi_k(\vec{r_i}_0) \tag{2.12}$$

Where Q_k is the charge induced on electrode k, q_i is the charge of the carrier i, $\vec{r_i}$ its position and ϕ_k the Ramo potential of electrode k. The Ramo potential is calculated by solving the Laplace's equation in the geometry of the detector while imposing a Dirichlet boundary condition at the electrodes, with $\phi = 1$ at the k'th electrode and 0 at the other present electrode and a Neumann boundary condition ($\vec{\nabla}\phi \cdot \vec{n} = 0$, $\vec{n}$ is the vector normal to the boundary) at the rest of the boundaries. This theorem can be applied to a variety of detection medium ranging from plasma to solid-state detectors. The presence of space charge do not influence the calculation of the Ramo potential Cavalleri [1971]; Gatti et al. [1987]

2.3 The Hybrid Planar Pixel Sensor

The planar pixel sensor (figure 2.7) consists of an array of small rectangular diodes built by implanting dopant in a Silicon wafer to form junctions. Lithography methods are used to create the individual pixels diodes and contact electrode. An implant and a metallization on the backside of the wafer is created with a dopant type opposite of the pixel's implant type. This create an ohmic contact. Bias is applied between each side of the wafer to deplete the sensor and create an electric field in the bulk of the sensor allowing the drift of free carriers generated by ionizing particles. The carrier cloud generated is localized in a small region around the particle track allowing to measure the particle position in the sensor using signal induced on the individual pixels. An integrated circuit, called a front-end, is also built with individual cells of signal lecture and digitization electronics matching the pixels on the planar sensor. The integrated circuits individual channels are coupled to the diodes using the bump-bonding technique. Each channel can then be read individually in a digital format to obtain the information on the position and energy of the detected particles. The assembly is then mounted on a PCB or a Flex-Hybrid containing the circuits

to bias the sensors and the integrated circuits and readout and transmit the acquired data. The final assembly is call hybrid Planar pixel sensor module and can be used to form large system of particle tracking used in large HEP experiments such as ATLAS.

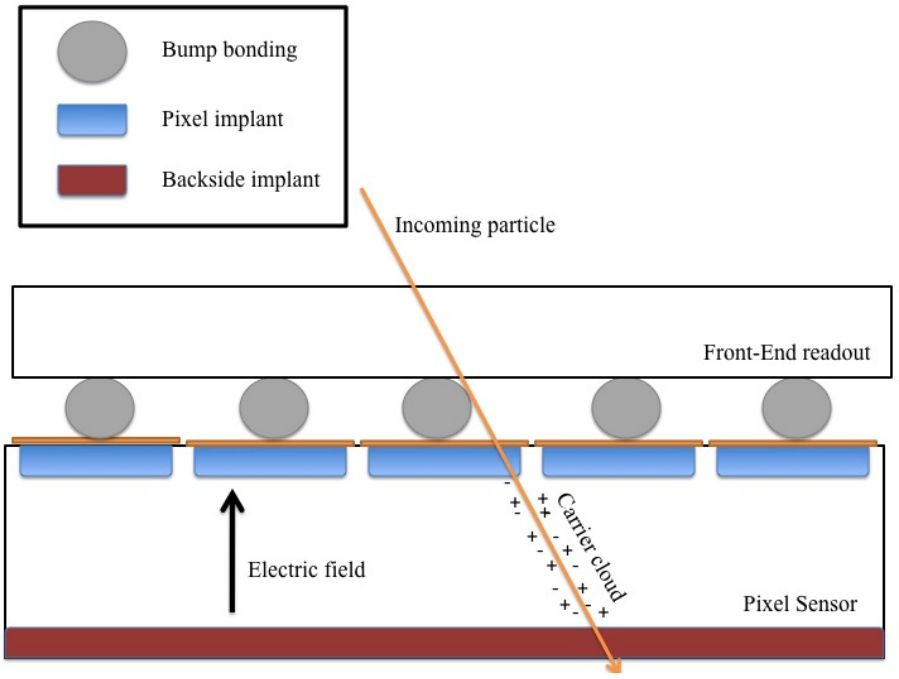

FIGURE 2.7 – Schematics of the hybrid planar pixel sensor.

2.4 Other Silicon sensors

In the recent years, new technologies have been developed to build pixel sensors for particle detection. The goal of these new technologies is to increase the signal formation speed, reduce inactive zones of the sensor, build thinner sensor and increase radiation hardness for applications where such characteristics are required. The two main new technologies are the 3D pixel sensor and the High Resistivity Monolithic Active Pixel Sensor (MAPS).

2.4.1 the 3D pixel sensor

The main difference between the planar pixel sensors and the 3D variety is the orientation of the electrode implant in the wafer. Through chemical etching techniques, deep holes are created in the wafer and implants are created on the surface of the holes, forming

p-type and n-type columns in the wafer. They are then filled with a conductive material to form the anodes and the cathodes. The bias is applied between the two type of columns and drift of the carriers occurs laterally, as shown in figure 2.8. For sensors with a pixel pitch smaller than the wafer thickness, this leads to a faster signal and smaller depletion voltage. The possibility to bias literally avoid the problem of high voltage distribution at edges present in planar pixel sensors, discussed in chapter 3 of this thesis, allowing for small inactive edges. Finally , the short drift distances of the carriers reduce the signal loss due to trapping during long charge drift makes the 3D sensors more radiation hard by design, since, as it will be discussed in the next section of this chapter, radiation damage induced charge loss by trapping of carriers in discrete energy levels present in the band-gap of the sensor's material.

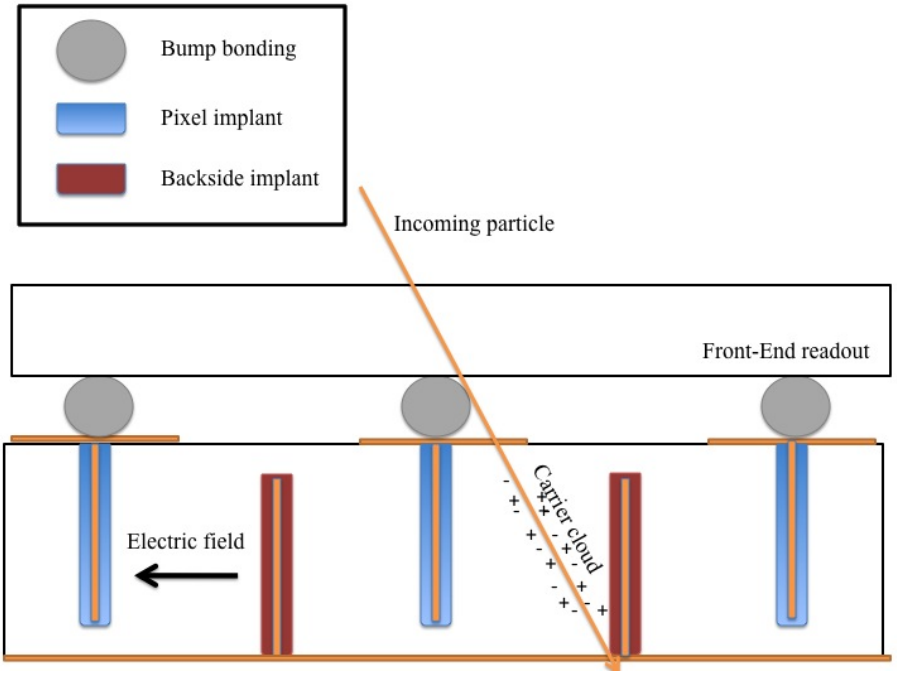

FIGURE 2.8 – Schematics of the hybrid 3D pixel sensor.

2.4.2 High Resistivity Monolithic Active Pixel Sensors (MAPS)

MAPS sensors are built on a single high resistivity silicon wafer where a low resistivity silicon layer have been grown by epitaxy. A small subsection of the pixel surface is occupied by a detection diode depleting in the high resistivity buried layer, while the rest of the

surface is occupied by CMOS electronics in the low resistivity bulk, forming the readout electronics of the diode, as shown in figure 2.9. A small electric field is present in the depleted region and a small signal is generated in the detection diode. The signal is then amplified and digitize on the same wafer by the readout electronics. The presence of the amplifier so close to the detection diode allows low noise operation even with the small signal produced by the passage of a particle. The presence of the electronics on the same wafer used for detection eliminated the need for a front-end integrated circuits and the small thickness of the epitaxial layer and detection layer (down to 50 μm) allows to build very thin sensors for low material budget applications.

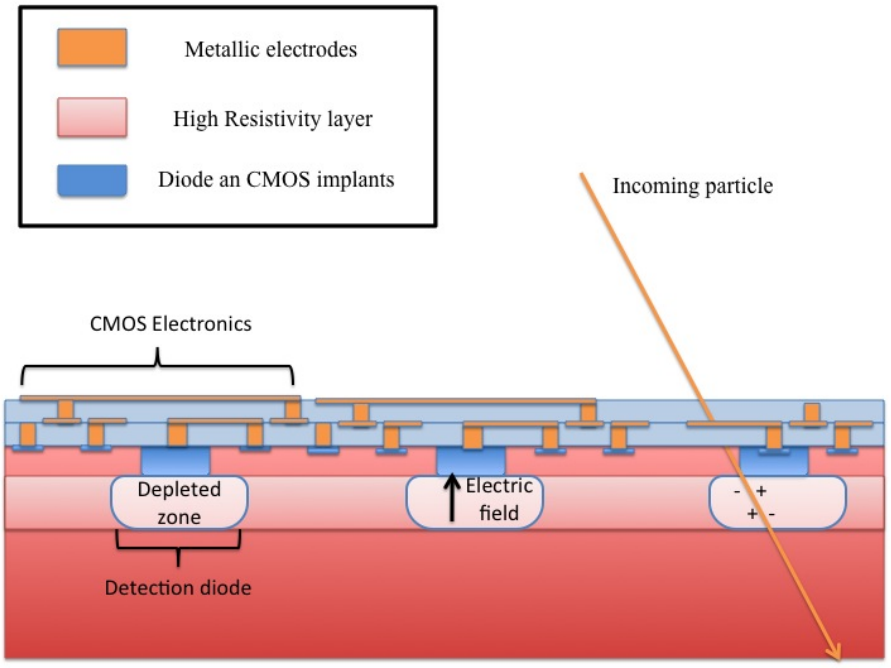

FIGURE 2.9 – Schematics of the High Resistivity Monolithic active pixel sensor (MAPS).

2.5 Radiation damage in Silicon sensors

Silicon sensors can be damaged by the exposure to radiation. Several effects need to be taken into account to design radiation hard sensors for use in harsh environment such as in ATLAS inner detector. Two kind of radiation damage are important in the case of silicon sensors : Non-ionizing and ionizing energy loss by particles interacting with the

sensor's material. Each effect lead to specific changes in the sensors operation conditions and electrical characteristics.

2.5.1 Non-ionizing Energy Loss (NIEL)

Exposure of planar pixel sensor to non-ionizing energy loss from protons, pions and neutrons modify its electrical properties in the following ways :

- Space-Charge Sign Inversion (SCSI)
- Modification of full depletion potential (V_{fd}) (high voltage operation after high-dose)
- Increased trapping
- Leakage current increase

NIEL is usually expressed, for silicon sensors, in 1 MeV neutron-equivalent by square centimeter, (n_eq/cm^2). The energy loss by exposure to different particle types and energies can be calculated by scaling the flux of the incoming particle on the sensor surface by the ratio between the NIEL in the bulk for that particle and the NIEL for a 1 MeV neutron. A large number of publication measuring the NIEL scaling factor for various type of particle is available (CITATION NIEL LHC).

SCSI effect was first predicted then measured experimentally Verbitskaya [2007]; Li and H. Kraner [1992]. It is expressed through an inversion of the space charge sign in the depleted region of silicon sensors. This inversion has been shown to be due to the introduction of electrically active defects in the bulk that compensate for the natively present defects. This leads to an apparent change of the bulk type, changing the wafer side where the high electric field is present and eventually leading to a complex distribution of space charge in the bulk leading to the formation of a high field region on both side of the silicon wafer ($N^+ - p - n - p^+$ structures). From equation 2.7, we can observe that an apparent charge in the bulk's acceptor or donor net quantity will also lead to a variation of the depletion voltage needed to fully deplete the silicon sensor. The steady introduction of these electrically active defects will eventually lead to an increase of the need depletion voltage and may limit the capacity to deplete the sensor completely.

Signal carriers are subject to recombination with the same probability as thermally generated carriers. The introduction of defects in the bulk will lead to a lower characteristic recombination time of the free carriers through these defects. If this time is of the order, or lower than expected collection time, it will lead to a reduction of the collected charge with regard to the expected value before the introduction of the defects. This radiation damage effect will lead to lower detection efficiency, reduced resolution, lower Signal to noise ratio and will force frequent recalibration of the sensor's readout electronics.

Finally, the traps in the band-gap are possible mediator for generation and recombination of carriers in indirect band-gap semiconductors. The addition of new trap in the sensor material will then lead to an increased probability of thermal emission of carriers leading to an increased leakage current. This represent an issue reducing the detector performance by increasing the noise and can lead to cooling problems and thermal runaway as the dissipated energy becomes more important. Finally, if the current leaking through the sensor is too important for the front-end readout out current compensation circuit capacity , it can lead to non-linear behavior of the electronics reducing the detector overall performances.

For a trap t, introduced by radiation or present in the original detector material, four processes can be enhanced : hole capture (R_h^t), hole emission (G_h^t), electron capture (R_e^t) and electron emission (G_h^t). Equations 2.13,2.14,2.15 and 2.16 (**?**) show the rate of each these processes as a function of the trap's capture cross-section ($\sigma_{p,n}^t$), thermal velocity (v_{th}), trap density (N_t), free carrier concentration (p, n),hole or electron emission probability ($\epsilon_{p,n}^t$) and Occupation probability of the trap (P_t).

$$R_h^t = v_{th,p}\sigma_p^t p N_t P_t \tag{2.13}$$

$$G_h^t = v_{th,p}\epsilon_p^t N_t (1 - P_t) \tag{2.14}$$

$$R_e^t = v_{th,n}\sigma_n^t n N_t (1 - P_t) \tag{2.15}$$

$$G_e^t = v_{th,n}\epsilon_n^t N_t P_t \tag{2.16}$$

At equilibrium, the sum all recombination and generation rates must equal 0 (equation 2.17). In this state, some concentration of defects can remain charged and modify the space charge distribution in the sensor, as seen in the SCSI effect. An increased trap density lead to bigger generation term and higher leakage current in reverse biased diode where recombination terms are kept low due to low free carrier density.

$$\sum_t G^t_{e,h} = \sum_t R^t_{e,h} \tag{2.17}$$

During collection time in the depleted zone of a reverse biased diode where carrier density is low, a quasi-static approximation, as shown in equation 2.18 can be used to determine the behavior of the signal's carriers during charge collection. This model supposes no carriers exchange between the different defects present, which is a valid approximation if defect density is low. The localized higher carrier density (n, p) in the charge cloud generated by the energy deposition of a particle, recombination terms are enhanced and lead to trapping of the signal if a large density of trap is present. A radiation damage increase, more trapping will occur and lead to lower charge collection efficiency.

$$\frac{dn, p}{dt} = \sum_t G^t_{e,h} - \sum_t R^t_{e,h} \tag{2.18}$$

For a distribution of carriers drifting in a reverse biased diode, one can compute the current induced on an electrode w using Ramo's field (Φ_w), as a function of generation/recombination rate, as shown in equation 2.20.

$$I_w(t) = \int_{volume} \rho(\vec{x}, \sum_t R^t_{e,h}(\vec{x}), \sum_t G^t_{e,h}(\vec{x}))\vec{\nabla}\Phi_w d\vec{x} \tag{2.20}$$

This equation is however complex to solve and one can approximate the collected charge by supposing a uniform distribution of traps, a constant electrical field and a punctual charge, neglecting generation of carriers. The recombination rate of the traps can be then expressed in term of the trap characteristic lifetime ($R_e, h = 1/\tau_t^{e,h}$). An average cha-

racteristic lifetime can be calculated using equation 2.21 and the collected charge can be expressed using equation 2.22.

$$\frac{1}{\tau} = \sum_t \frac{1}{\tau_t} \tag{2.21}$$

$$Q_f = \int_{t_0}^{t_f} Q_0 \mu_{e,h} \vec{E} e^{-t/\tau} \vec{\nabla} \Phi_w(Q_0 \mu_{e,h} \vec{E} t) dt \tag{2.22}$$

The hadronic interactions of particles with the atoms of the crystal lattice transfers to them part of their kinetic energy and displaces them from their original position, creating disorder in the crystalline structure. The displaced atoms can be moved to interstitial space in the lattice, forming a defect, called interstitial defect, than can become electrically active and modify the band structure of the silicon. The vacancies in the lattice left by the knocked-off atom can also create an electrically active defect called the vacancy defect.

Moreover, the pre-exisisting defects and dopants in the silicon bulk can interact with the radiation induced defects to form more complex hybrid defects with different electrical behavior. The ROSE Lindstrom and al. [2001a,b]; Ruzin [2000] and RD50 CERN collaboration Bruzzi and Moll [2003]; Luukka [2004]; Campabadal. et al. [2005]; Bruzzi and Moll [2005]; Moll and Mara [2008] have worked to identify the defects that are important to understand the effects of non-ionizing radiation damage in silicon . The main important defects introduced in silicon by irradiation can be found in table 2.2. The introduction rate of these different defects vary with the type and energy of the particle causing the damage, the present concentration of Oxygen in the bulk and of the thermal history of the silicon sample. Defect engineering can be performed by favoring the formation of non electrically active defects such as the $(V - O_{2i})$ defect which is enhanced by the presence of Oxygen dimers (O_{2i}). Oxygenated high resistivity silicon exhibit a high concentration of such dimer and therefore can substain higher radiation doses before effects detrimental to the operation of the planar pixel sensor becomes significant.

The modeling of the complex chemistry of defects in irradiated silicon can be quite complex and unpractical for the modeling of irradiated pixel sensors. However simple parametrization reproducing well the different known effects observed in silicon has been

TABLE 2.2 – Important defects introduced by NIEL in silicon (Lutz [2007]; Campabadal. et al. [2005])

Defect type	Charge state	Energy level (eV)
Interstitial (I)	I^-	$E_C - 0.39$
	I^0	
	I^-	$E_V + 0.4$
Vacancy (V)	V^{--}	$E_C - 0.09$
	V^-	$E_C - 0.4$
	V^0	
	V^+	$E_V + 0.05$
	V^{++}	$E_V + 0.13$
Divacancy (V_2)	V_2^{--}	$E_C - 0.23$
	V_2^-	$E_C - 0.39$
	V_2^0	
	V_2^+	$E_V + 0.21$
A-Center (V-O)	$(V-O)^-$	$E_C - 0.18$
	$(V-O)^0$	
Divacancy Oxygen complex ($V_2 - O$)		
Vacancy Oxygen dimer complex ($V - O_{2i}$)	$(V - O_{2i})^0$	

developped in the recent years. A deep acceptor and a deep donor are introduced in the bulk to account for space charge sign inversion (SCSI), double junction effects Verbitskaya [2007]; Li and H. Kraner [1992] and leakage current increase Verbitskaya [2007]; Li and H. Kraner [1992]; Menichelli et al. [1999]; Eremin et al. [2002]. In addition, to account for trapping and recombination of carrier induced by radiation damage, a shallow hole and electron trap must be added. The model we used is shown in tables 2.3 and 2.4 , based on the latest results from RD50 collaboration Moll and Mara [2008] and work of several groups Moscatelli and al. [2002, 2004]; Petasecca et al. [2006].

TABLE 2.3 – n-type radiation damage model

Defect's energy (eV)	Introduction rate (cm^{-1})	Electron capture cross-section (cm^{-2})	Hole capture cross-section (cm^{-2})
$E_c - 0.42$	13	2.2e-15	1.2e-14
$E_c - 0.53$	0.08	4e-15	3.5e-14
$E_c - 0.18$	100	1e-14	1e-16
$E_v + 0.36$	1.1	2e-18	2.5e-15

TABLE 2.4 – p-type radiation damage model

Defect's energy (eV)	Introduction rate (cm^{-1})	Electron capture cross-section (cm^{-2})	Hole capture cross-section (cm^{-2})
$E_c - 0.42$	1.613	2.e-15	2e-14
$E_c - 0.46$	0.9	5e-15	5e-14
$E_c - 0.10$	100	2e-15	2.5e-15
$E_v + 0.36$	0.9	2.5e-14	2.5e-15

These parameters must be adjusted using a fit method to determine adequate introduction rates, level and capture cross-section for each type of silicon used.

A simpler parametric model has been developed by the ROSE and RD50 collaboration to evaluate the evolution of leakage current, average trap characteristic lifetime and net dopant/defect concentration in irradiated sensors. The Variation of leakage current density in the bulk of a depleted sensor is parametrized following equation 2.23

$$\frac{\Delta I_{vol}}{V} = \alpha\Phi \tag{2.23}$$

Where I_{vol} is the volume generated current, V the bias potential, α the leakage damage constant and Φ the exposed fluence in n_{eq}/cm^2. The average trap characteristic lifetime can be also be expressed as a function of fluence as shown in equation 2.24, where τ_{t0} is the original trapping time.

$$\frac{1}{\tau_t(\Phi)} = \frac{1}{\tau_{t0}} + \beta\Phi \tag{2.24}$$

Finally, the net dopant/defect concentration is expressed following equation 2.25, where N_{D0} is the initial donor concentration, N_{A0} the initial acceptor concentration and N the net dopant concentration. From N, it is possible to compute the depletion potential following equation 2.7. Acceptor removal and donor creation have not been observed experimentally, explaining the absence of such term in this equation.

$$N(\Phi) = N_{D0}e^{-c\Phi} - N_{A0} - b\Phi \tag{2.25}$$

Table **??** show typical value for the radiation damage constants of this model.

TABLE 2.5 – Typical radiation damage constants Wunstorf et al. [1992]

constant	value
α	$8.0 \times 10^{-17}\ Acm$
β	$0{,}24 \times 10^{-6}\ cm^2 s^{-1}$
c	$3.54 \times 10^{-13}\ cm^2$
b	$7.94 \times 10^{-2}\ cm^{-1}$

2.5.2 Ionizing energy loss

Silicon dioxide present at the surface is the main material damaged by ionizing energy loss . The dose of ionizing energy loss radiation damage is usually expressed in Rad, which represent 6.24×10^{10} MeV of ionizing energy deposition per kilogram of material.

SiO2's Oxygen valence electrons present at the interface and uncompensated by a Silicon atom create local traps for holes, as shown in figure 2.10. Holes from electron-hole pairs generated by ionizing particles crossing the oxide can be trapped in this layer. Electrons have higher mobility ($20\ cm^2/Vs$) than holes ($2 \times 10^{-5}\ cm^2/Vs$) in SiO2 and collect rapidly while holes accumulates in the traps present near the interface Rossi et al. [2006]. The electrical field created by this sheet of positive charge attracts silicon's free electrons that then for a compensating layer of free carrier at the Si-SiO2 interface. Few carriers can cross the interface potential barrier by tunneling and recombine with their opposite carrier, leaving the charge layer, called inversion layer, almost permanently at the interface.

The charge density at the interface is known to vary almost linearly with exposed fluence from $10^{11}\ cm^{-2}$ to $10^{12}\ cm^{-2}$ between 0 and $1 \times 10^8\ Rad$, usually equivalent in ATLAS inner detector to exposition to a NIEL of 0 to $1 \times 10^{15}\ n_{eq}/cm^2$. We then consider the charge layer to be saturated for higher fluences, as observed experimentally Wustenfeld [2001]. Oxide charge saturation concentration is process dependent Nicollian and Brews [2002] so the saturation fluence and charge concentration can be chosen for modelisation

to be coherent with the data presented in literature.

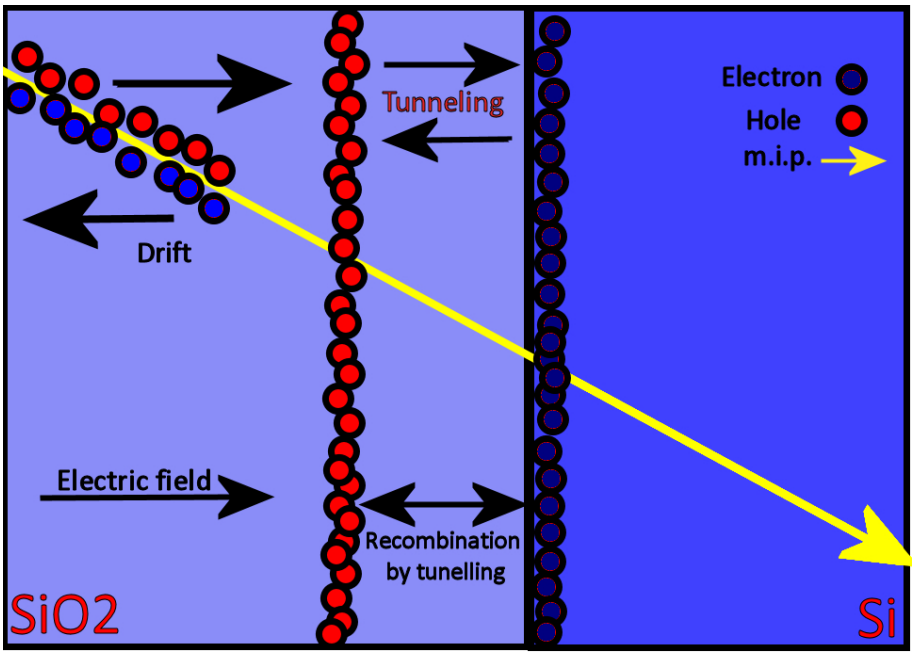

FIGURE 2.10 – Schematics of radiation damage effect at the silicon-silicon dioxide interface in silicon sensors.

The presence of this electron layer at the interface can form a conductive path between different electrodes, increasing crosstalk and leading to unwanted parasitic leakage path in the sensor. Mitigation methods to prevent this effect will be presented in next chapter.

Chapitre 3

TCAD Simulation models and experimental validation

texte...

3.1 Principles of TCAD simulation

texte...

3.1.1 The physics models

texte...

3.1.2 Boundary conditions

texte...

3.1.3 Process simulation

3.1.3.1 Processing step of silicon diodes

3.1.3.2 Large scale process simulation

texte...

3.1.4 Device simulation

texte...

3.2 The Multi-Guard Ring structure

3.2.1 Principles of guard ring structures

3.2.2 Optimization of guard ring structures for radiation hardness

3.2.3 Study of guard ring structure in slim edges planar pixel sensors

3.3 The charge amplification mechanism in highly irradiated silicon sensors

3.4 Experimental validation

3.4.1 Doping profile measurements

3.4.2 Guard Ring measurements

3.4.3 Current versus Bias characteristics

3.4.4 Depletion Potential measurements

3.4.5 Experimental evidence of the charge amplification mechanism

Chapitre 4

From TCAD simulation and experimental data to digitization

texte...

4.1 Monte Carlo charge transport simulation

4.2 Planar pixel sensor digitization

4.2.1 Implementation in GEANT4 simulation of the FEI3 and FEI4 digitization

4.3 Test beam validation of TCAD simulation

4.3.1 Validation of the digitization model

4.3.2 Edge effects

4.3.3 Charge amplification

Chapitre 5

Physics motivations

texte...

5.1 $H->\tau\tau$ phenomenology

5.2 IBL Simulation

5.2.1 Thinning effects

5.2.2 Slim edges effects

Chapitre 6

Perspective for future Radiation-Hard Silicon Planar Pixel sensors

texte...

6.1 3D electronics front-end read-out

6.2 Charge amplification pixel structures

texte...

Conclusion

Ici la conclusion...

Bibliographie

M. Bruzzi and M. Moll. Rd50 status report 2002/2003 rd50 : Radiation hard semiconductor devices for very high luminosity colliders. *CERN*, 2003. 38

M. Bruzzi and M. Moll. Rd50 status report 2005 : Radiation hard semiconductor devices for very high luminosity colliders. *CERN*, 2005. 38

F. Campabadal., M. Bruzzi, and M. Moll. Rd50 status report 2004 : Radiation hard semiconductor devices for very high luminosity colliders. *CERN*, 2005. 13, 38, 39

D. M. Caughey and R. E. Thomas. Carrier mobilities in silicon empirically related to doping and field. *Proc. IEEE*, 55(12) :2192–2193, 1967. 25

G. Cavalleri. Extension of ramo's theorem as applied to induced charge in semiconductor detectors. *Nucl. Instr. and Meth.*, 33 :137–140, 1971. 31

V. Eremin, E. Verbitskaya, and Z. Li. The origin of double peak electric field distribution in heavily irradiated silicon detectors. *Nucl. Instrum. Meth. A*, 476(3) :556 – 564, 2002. ISSN 0168-9002. doi : DOI:10.1016/S0168-9002(01)01642-4. 39

E. Gatti, A. Longoni, P. Rehak, and M. Sampietro. Dynamics of electrons in drift detectors. *Nuclear Instruments and Methods in Physics Research A*, 253 :393–399, January 1987. doi : 10.1016/0168-9002(87)90522-5. 31

Frank Hartmann. *Evolution of silicon sensor technology in particle physics*. Springer, 2009. ISBN 9783540250944. URL `http://www.worldcat.org/isbn/9783540250944`. 21

Glenn F. Knoll. *Radiation Detection and Measurement*. Wiley, 4 edition, August 2010. ISBN 0470131489. URL `http://www.amazon.com/exec/obidos/redirect?tag=citeulike07-20&path=ASIN/0470131489`. 27

Z. Li and H. H. Kraner. Fast neutron radiation damage effects on high resistivity silicon junction detectors. *J. Electronic Materials*, 21(7) :701–705, 1992. 35, 39

G. Lindstrom and al. Developments for radiation hard silicon detectors by defect engineering–results by the cern rd48 (rose) collaboration. *Nucl. Instrum. Meth. A*, 465 : 60 – 69, 2001a. ISSN 0168-9002. doi : DOI:10.1016/S0168-9002(01)00347-3. 38

G. Lindstrom and al. Radiation hard silicon detectors–developments by the rd48 (rose) collaboration. *Nucl. Instrum. Meth. A*, 466(2) :308 – 326, 2001b. ISSN 0168-9002. doi : DOI:10.1016/S0168-9002(01)00560-5. 38

Gerhard Lutz. *Semiconductor Radiation Detectors : Device Physics (Accelerator Physics)*. Springer, May 2007. ISBN 3540648593. URL `http://www.worldcat.org/isbn/3540648593`. 13, 28, 39

P. Luukka. Status of defect engineering activity of the rd50 collaboration. *Nucl. Instrum. Meth. A*, 530 :152–157, 2004. 38

M.N. Mazziotta. Electron-hole pair creation energy and fano factor temperature dependence in silicon. *Nuclear Instruments and Methods in Physics Research Section A : Accelerators, Spectrometers, Detectors and Associated Equipment*, 584 (2-3) :436 – 439, 2008. ISSN 0168-9002. doi : DOI:10.1016/j.nima.2007.10.043. URL `http://www.sciencedirect.com/science/article/B6TJM-4R29FFR-4/2/4e64eabfcf36ab09a0118634a761b37e`. 29

D. Menichelli, M. Bruzzi, Z. Li, and V. Eremin. Modelling of observed double-junction effect. *Nucl. Instrum. Meth. A*, 426 :135–139, April 1999. doi : 10.1016/S0168-9002(98)01482-X. 39

M. Moll and B. Mara. Rd50 status report 2007 - radiation hard semiconductor devices for very high luminosity colliders. *CERN*, 2008. 38, 39

F. Moscatelli and al. An enhanced approach to numerical modeling of heavily irradiated silicon devices. *Nucl. Instrum. Meth. B*, 186(1-4) :171–175, January 2002. 39

F. Moscatelli and al. Comprehensive device simulation modeling of heavily irradiated silicon detectors at cryogenic temperatures. *IEEE Trans. Nucl. Sci.*, 51(4) :1759–1765, 2004. ISSN 0018-9499. 39

E. H. Nicollian and J. R. Brews. *MOS Physics and Technology.* Wiley-Interscience, 2002. 41

M. Petasecca, F. Moscatelli, D. Passeri, G.U. Pignatel, and C. Scarpello. Numerical simulation of radiation damage effects in p-type silicon detectors. *Nucl. Instrum. Meth. A*, 563(1) :192 – 195, 2006. ISSN 0168-9002. doi : DOI:10.1016/j.nima.2006.01.093. 39

Yu Y. Peter and M. Cardona. *Fundamentals of Semiconductors, 3rd Edition.* Springer, 2003. 24, 25

Simon Ramo. Currents induced by electron motion. *Proceedings of the I.R.E.*, 27 :584, 1939. 31

L. Rossi, P. Fischer, T. Rohe, and N. Wermes. *Pixel Detectors : From Fundamentals to Applications.* Springer, 2006. 41

A. Ruzin. Recent results from the rd-48 (rose) collaboration. *Nucl. Instrum. Meth. A*, 447 (1-2) :116 – 125, 2000. ISSN 0168-9002. doi : DOI:10.1016/S0168-9002(00)00179-0. 38

V. Verbitskaya. Concept of double peak electric field distribution in the development of radiation hard silicon detectors. *Nucl. Instrum. Meth. A*, 583(1) :77 – 86, 2007. ISSN 0168-9002. doi : DOI:10.1016/j.nima.2007.08.228. 35, 39

R. Wunstorf, M. Benkert, N. Claussen, N. Croitoru, E. Fretwurst, G. Lindstrom, and T. Schulz. Results on radiation hardness of silicon detectors up to neutron fluences of 1015 n/cm2. *NIMA*, 315(1-3) :149 – 155, 1992. ISSN 0168-9002. doi : DOI:10.1016/0168-9002(92)90696-2. URL `http://www.sciencedirect.com/science/article/B6TJM-470F673-17G/2/ce7027b412713b3145838a395dcbc579`. 13, 41

Jens Wustenfeld. *Characterisation of ionisation induced surface effects for the optimisation of silicon detectors for particle physics applications.* PhD thesis, 2001. 41

Annexes

Annexe A

Doping profile measurements

Annexe B

Clean room experimental setup

Annexe C

The ALLPix Simulation Software

Glossaire

– $CNAM$: Conservatoire National des Arts et Métiers

le cnam

Prénom NOM

TITRE
TITRE

sous-titre

le cnam

Résumé :
le résumé

Mots clés :
Mots clés

Abstract :
abstract

Keywords :
keywords